Geosci. Instrum. Method. Data Syst. Discuss., 4, 627–651, 2014
www.geosci-instrum-method-data-syst-discuss.net/4/627/2014/
doi:10.5194/gid-4-627-2014

Geoscientific Instrumentation Methods and Data Systems Discussions
Open Access

A high dynamic radiation measurements instrument: the Bolometric Oscillation Sensor (BOS)

P. Zhu[1], M. van Ruymbeke[1], Ö. Karatekin[1], J.-P. Noël[1], G. Thuillier[3], S. Dewitte[2], A. Chevalier[2], C. Conscience[2], E. Janssen[2], M. Meftah[3], and A. Irbah[3]

[1]Royal Observatory of Belgium, Av. Circulaire 3, 1180 Bruxelles, Belgium
[2]Royal Meteorological Institute of Belgium, Av. Circulaire 3, 1180 Bruxelles, Belgium
[3]LATMOS, 4 place Jussieu 75252 Paris CEDEX 05, France

Received: 5 August 2014 – Accepted: 5 November 2014 – Published: 3 December 2014

Correspondence to: P. Zhu (zhuping@oma.be)

Published by Copernicus Publications on behalf of the European Geosciences Union.

Abstract

The bolometric oscillation sensor (BOS) is a broadband radiation measurement instrument onboard the PICARD satellite that has been active between 2010 and 2014. The main detector is a thermistor attached black coated surface, which was permanently exposed to space without any optical and aperture accessories. The temperature measurements are used within a transfer function to determine variations in incoming solar irradiance as well as the terrestrial radiation. In the present article, the measurement principle of BOS and its transfer function are presented. The performance of the instrument is discussed based on laboratory experiments and space observations from the PICARD satellite. The comparison of the short term variation of Total Solar Irradiance (TSI) with absolute radiometers such as VIRGO/SOHO and TIM/SORCE over the same period of time, suggests that BOS is a relatively much simpler but very effective sensor to monitor electromagnetic radiation variations from visible to infrared wavelengths.

1 Introduction

The SOlar VAriability experiment for the PICARD mission (SOVAP) is one of the three instruments constituting the solar payload of CNES's microsatellite PICARD (Thullier et al., 2006). It is composed of a DIARAD type absolute radiometer (Dewitte et al., 2004) and the bolometric oscillation sensor (BOS) (van Ruymbeke et al., 2010, 2011), which are measuring the incoming radiation with a sampling frequency of 180 s and 10 s, respectively. The main requirement for BOS was to provide stable and precise measurements of the incoming electromagnetic radiation over the broad spectrum with a high 10 s cadence.

The absolute value of the solar irradiance was not requested a priori during the designing phase since the BOS was collocated to the DIARAD absolute radiometer, which is providing sound TSI measurement with rich space heritage (Mekaoui et al.,

GID
4, 627–651, 2014

2010). The big challenge was rather to develop a small compact instrument that could continuously monitor the variation of the solar irradiance as well as of the terrestrial radiation with a high precision. To achieve this objective, the BOS team has developed an innovative design that enhances the performance of the instrument by reducing the electronic common-mode and the ambient thermal noise.

The PICARD microsatellite with the BOS onboard, was successfully launched on 15 June 2010. PICARD is a technological demonstration mission with a nominal duty cycle of two years. Following two years of operation, the mission was extended for one and a half year. PICARD has three experiments; SODISM (Meftah et al., 2014a) measures the diameter of the Sun, while PREMOS (Schmutz et al., 2013), and the SOVAP (Zhu et al., 2010; Meftah et al., 2014b) measure the total and spectral solar irradiance. The science payloads (Fig. 1 left) and the SOVAP instrument package is showed in (Fig. 1 right). The BOS as a part of the SOVAP experiment, has acquired data quasi-continuously over the three and half year mission duration. BOS data are archived and publically available on the website (http://picard-bos.oma.be).

In the next section the measurement principle of BOS and its geometry are presented, Reduction of the electronic common-mode and background ambient thermal noise is discussed in the Sect. 3. The laboratory experiment and the flight performance of the instrument are respectively presented in Sects. 5 and 6. The space observation results are then compared with the absolute radiometers VIRGO/SOHO and TIM/SORCE.

2 Operating principle and geometry

The measurement principle of the BOS is a combination of a thermistor based bolometer and a pyrometer. The basic geometry is a cylinder where the heat flux measurement is realized through temperature measurements at thermal nodes (Fig. 2 left). The team has tested number of prototypes before opting for this flying model (Fig. 2 right) (van Ruymbeke, 2006).

GID
4, 627–651, 2014

The sensing unit is composed of two pieces of mass m_1 and m_2. It is made of aluminum, to which a special space qualified treatment (alodyne 1200) was applied before the final chemical coating. The surface of m_1 is painted in black and the m_2 is painted in white with MAP© coating. The mass m_1 is then connected to m_2 through a thin shunt at the bottom of m_2. It is thermal insulated from m_2 with multi-layer-isolation. The length of the shunt was determined by computer simulations (Martinez, 2007).

The working principle of BOS is quite straight forward. The light mass (m_1) is absorbing and reemitting a broadband wavelength electromagnetic radiation from space. The heavier mass (m_2) is absorbing less energy and reemitting most energy caught by m_1 and m_2 back to space.

According to the thermal node analysis method, the thermal network of BOS is approximated by the temperature at two diffusion nodes T_1 and T_2. Mathematically, the temperature of the diffusion node is modeled by the expression (K&K Associate, 2000):

$$\Sigma Q - C\frac{\mathrm{d}T}{\mathrm{d}t} = 0 \tag{1}$$

with ΣQ, the sum of the thermal energy of the network, and C, the thermal capacitance. The instrument is thermally insulated from the outside with a high thermal resistance Vespel® layer. Supposing a constant temperature of the environment, the diffusion node can be approximated by,

$$\Sigma Q = \alpha s_1 Q_{\mathrm{in}} - \epsilon s_1 \sigma T_1^4 - K\Delta T \tag{2}$$

where, α and ϵ are the absorption and emissivity coefficients of the black coating, Q_{in}, the incoming electromagnetic radiation, s_1, the surface area of mass m_1, σ the Stefan-Boltzman coefficient, $K = kA/L$, the thermal conductance, k, thermal conductivity of the shunt, A, L, surface area and length of the shunt, $\Delta T = T_1 - T_2$, the difference between T_1 the temperature measured under the black surface, and T_2, the temperature at the bottom end of the shunt (Fig. 2). The effect of electronic common-mode as well as the background ambient thermal noise are discussed in the next section.

GID
4, 627–651, 2014

From Eqs. (1) and (2), we can find a numerical solution of Q_{in} with the values of two temperature measurements:

$$Q_{in} = \frac{1}{\alpha s_1}\left(\epsilon s_1 \sigma T_1^4 + K\Delta T + C\frac{dT_1}{dt}\right) \quad (3)$$

Since the sensing surface of m_1 is directly exposed to space with a hemispherical field of view (HFOV), it is absorbing all electromagnetic radiation by principle. We use the Mini BetaCurve polymide NTC thermistor component as temperature detectors. These components were calibrated by measurement specialities. The thermistor resistance at 25 °C is 100 KΩ. The tolerance of the beta value is ±0.5 % at 25 °C (Measurements technical specialties® datasheet (Measurements, 2005)). Two electronic interfaces (EI) are separately connected to each thermistor. The V2F digital counting of each EI has a 120 dB dynamic bandwidth covering the T_1 working temperature range between −30 °C and 60 °C. The instrument is designed to be automatically off when the T_1 is out of this range. With such a large dynamic range, the resolution of the temperature measurement can theoretically reach 90 micro degree ($\frac{90}{10^6}$).

3 Reducing the electronic common-mode and background ambient thermal noise

The common-mode is usually indicating the noise induced by the amplifier of electronics. Here, it is referred to as the electronic common mode (ECM).

In order to limit the overheating by Joule effect, two resistances (74 KΩ for T_1 and 82 KΩ for T_2) are wired in series with NTC thermistors. The amplifier is separately applied to the output voltage of the first thermistor and to the voltage difference between the first and the second thermistor. This configuration is essentially increasing the resolution of temperature difference measurements and reducing the ECM by a common electronic interface rather than individually counting the output of two NTC thermistors (van Ruymbeke et al., 2010).

GID
4, 627–651, 2014

The instrument package was installed at the front sun-pointing panel of PICARD satellite and fixed with six screws. Each screw was rounded by a layer of Vespel®, which has a very low thermal conductivity coefficient ($0.005\,W\,cm^{-1}\,K^{-1}$) (Vespel technical Information Miller, 2000). The mass ratio between m_2 and main sensing unit m_1 is as high as 200. In addition, the energy absorbed by the black coated surface s_1 is two times higher than the white painting surface m_2 due to its strong reflectivity to visible radiation (Zhu et al., 2012). All these factors guarantee that the heat flux direction is from the main detector m_1 along the isolated shunt towards the junction between the shunt and m_2 during the Sun observation nominal phase. The surrounding ambient thermal noise is damped by the heat sink (m_2). The temperature measured at T_2 has been slowly changing over the mission and can be considered as a stable reference for short period thermal modulation.

4 Laboratory thermal vacuum test

The laboratory experiments were conducted with the spare Flight Model (FM) of BOS. The complete instrument was installed inside a vacuum tank. Since the model is connected to the inner wall of the vacuum tank through a support, the measurements are sensitive to the temperature of environment due to the thermal conductivity between the supporting mass of BOS and the vacuum tank. Therefore, it is important to do the experiments in a temperature controlled room. The experiments are realized in a thermally controlled room designed originally for astronomy photo disk digitizing. A climatisation installation delivered by Becker Reinraumtechnik® regulates the clean room to a constant air temperature of $20 \pm 0.05\,^{\circ}C$ and to a relative air humidity of $50 \pm 1\,\%$. (J.-P. De Cuyper, personal communication, 2014). A Labsphere Uniform Source Integrating Spheres is selected as radiation source (Labsphere PB-13019-000 Labsphere, 2005). The inner sphere of Labshpere is coated with Labsphere's highly reflective and durable Spectraflect® coating, it is producing a very homogenous UV-VIS-NIR radiation. The radiation source generated by Labshpere arrived at the front transparent

GID
4, 627–651, 2014

optical window of the vacuum tank after passing through a one centimeter aperture. The source is set to be automatically ON/OFF for eight measurement cycles. The duration of each measurement cycle is 99 min, which is approximately the orbital period of PICARD (Fig. 3a).

The T_1 and T_2 temperatures were recorded with a period of 10 s for the 8 repeated measurement cycles. The mean value and the SD (1σ) of T_1 is 294.897 ± 0.007 K, T_2 is 294.480 ± 0.004 K and the temperature difference ($T_1 - T_2$) is 0.423 ± 0.001 (Fig. 3b and c). The flux is calculated with Eq. (3) from the measurements of T_1 and T_2. The mean and SD of the flux is $472.8 \pm 0.1\,\mathrm{W\,m^{-2}}$. The 1σ value of temperature is at the level of miliKelvin, and that of the heat flux is about one tenth of $\mathrm{W\,m^{-2}}$ (Table 1). The signal shows a clear diurnal cycle variation in temperature and more evidently in flux (Fig. 3d).

5 Observations from space

The BOS sensor onboard the PICARD microsatellite was switched on in 28 June 2010. It has been continuously recording since then with a 10 s cadence. The total duty cycle of BOS observation is 1278 days. The complete space acquired level 2 data set in $\mathrm{W\,m^{-2}}$ is plotted at (Fig. 4a). The global data set is categorized according to the physical origin of the signal (Fig. 4b). The Nominal mode represents the data when the sensor is only receiving the solar and terrestrial radiation at an altitude around 725 km. During satellite occultations, the BOS sensor is looking through the upper atmosphere to the Sun until its vision is completely blocked by the Earth. This happened every year between the beginning of November and mid February.

MDO (Mode DistOrsion) represents the distortion mode of the satellite, during which the satellite was rotating clockwise along its Sun pointing axis. MES (ModE Stellaire) is the star pointing mode, in which, the sensing unit was pointing to a star in the deep space. The observations during MES are important for the calibration of all payload instruments. During the entire PICARD life time, there has been in total 22 MES

GID
4, 627–651, 2014

operations. We consider 17 of them for the inflight calibration of the BOS, excluding those with abnormal positive minimum, observed inside the occultation period of 2013. The cause of the anomaly is still under investigating.

Contrarily to the laboratory experiment, the temperature is measured around the minimum value during MES (Fig. 5a), because it is like a OFF/ON of radiation source and the laboratory experiment is a ON/OFF process of light. When the MES was started, the senor was passed a process.

During the MES, at the beginning, the sensor is still receiving solar energy. When the satellite is turning away from the sun to a star, the energy is gradually decreased until it does not receive the solar energy at all. The small valley around June to July in the records of T_1 and T_2 (Fig. 5b) and the corresponding plateau presented in (Fig. 5c), is due to the variation of solar and terrestrial radiation modulated by the Sun–Earth orbit distance change. Such effects is reduced by normalizing the calibrated flux in a unit distance 1 AU and correct velocity effects (Fig. 5d).

From 17 MES events, the mean value and the SD of T_1 is 305.3 ± 0.13, T_2 is 307.4 ± 0.13 K and $(T_1 - T_2)$, -2.356 ± 0.006 K, the value of the calibrated flux F is $1369.7 \pm 1.68\,\mathrm{W\,m^{-2}}$ (Table 2). The uncertainties of T_1 and T_2 are two orders and the flux F is one order higher than during the laboratory experiment. Only the difference temperature $T_1 - T_2$ shows a similiar level error budget than the results of laboratory experiment (Table 1).

The variation of the flux received by BOS was modulated by the Sun–Satellite distance which can be corrected using the knowledge of the position and attitude of the satellite. The BOS with its hemispherical field of view has been receiving both solar and terrestrial radiation above top of the atmosphere (TOA) which can not be separated easily. After normalizing the flux of MES to 1 AU, the decreasing radiative flux with time can be associated with the change in instrument sensitivity (Fig. 5d). The variation of the flux with time is calculated both from MES and from the global data set. Its linear fits is represented in Fig. 6. The former analysis yields to a loss of $-16.5\,\mathrm{W\,m^{-2}\,yr^{-1}}$ as the sensitivity decrease by 5 % over the whole mission, while the latter suggests a loss

GID
4, 627–651, 2014

rate of $-17.1\,W\,m^{-2}\,yr^{-1}$. Both results are in agreement within the 95% confidential level (Fig. 6).

6 Lambertian performance

The BOS has a hemispherical field of view (HFOV) and the detector is directly exposed to space without any optical or aperture accessories. The Lambertian performance is studied using the part of data obtained during MES, when the satellite is slowly turning away from Sun pointing axis to a star in deep space. We stacked all 17 MES records of descending phases, then we removed the mean value and normalized the stacking results to unity (Fig. 7a).

A set of rotational angles were obtained by inverting the result with a cosine function. The first derivatives of angles (α) gave the angular velocities of the motion (degrees/10 s). If the detector has a cosine response to the incoming radiation, the angular velocities distribution should be close to the true rotation of the spacecraft. Since the angular motion of the spacecraft was precisely controlled by the Attitude Determination and Control (ADCS) of PICARD, the angular velocity of PICARD is known in advance. Two different sets of angular velocity are plotted together in (Fig. 7b). The angular velocity from BOS is well following the true motion of the satellite. The cross-correlation coefficient between them is 99.2%. Thus the instrument has a Lambertian response to the incoming radiation. As a consequence, the total radiation emitted by the sun is equal to measured flux multiplied the cosine of the pointing angle. In case of PICARD, the pointing accuracy is better than 0.1° (Meftah et al., 2014b). For the radiation of Earth's origin, a correction factor has to be applied according to Lambert's cosine law.

GID
4, 627–651, 2014

7 Preliminary comparison with absolute radiometers

The variation of TSI is obtained after normalizing to 1 AU, correcting orbital velocity effects (Fröhlich et al., 1997) and removing the terrestrial radiation by seven days running mean. Since it is difficult to find a physical model of terrestrial radiation, which could be directly applied to the records, we used the running average to remove the daily variation induced by terrestrial radiation. Several different window lengths have been tested, the 7 days is selected because it yields stable results for the solar radiation and terrestrial radiation. For the solar radiation, we judge the results by comparing it with the satellite-sun distance modulation. The terrestrial radiation is then projected on a one degree by one degree map to be compared with CERES product. The details about these higher level product will be discussed in details in the future works.

We compared the variation of TSI with data of VIRGO/SOHO (Fröhlich et al., 1997) and TIM/SORCE (Kopp et al., 2011) over same period. VIRGO is a TSI composite from two absolute radiometer the PMO6V and DIARAD from SOHO. The TIM/SORCE is another total solar irradiance measurement, which is providing a new lower value of the solar constant. The variation of TSI is computed after removing the mean value of each individual data set. The sampling rate of VIRGO and TIM is linearly interpolated to 10 s to match the cadence of BOS. Figure 8 shows the short term variation of total solar irradiance from the three independent experiments. The cross-correlation between VIRGO and TIM is 97.5 %. The value for VIRGO-BOS is 60.3 % and TIM-BOS is 62.3 %. The BOS is following fairly well the TSI evolution of VIRGO/SOHO and TIM/SORCE assessing the capability of BOS to measure the TSI. The contribution of the terrestrial radiation, on the other side is more difficult to estimate due to the variation with time of the angle between the source and the sensor.

GID
4, 627–651, 2014

8 Conclusions and discussions

The Bolometric Oscillation Sensor has worked in space for 3.5 years. The sensibility of the absolute temperature measurements have been determined in laboratory to be in the order of 10^{-3}. In flight data rather suggest uncertainties in the order of 0.1 K, which is two orders higher than the laboratory results. The 1σ value of flux determination is $1.6\,W\,m^{-2}$, it is about ten times of laboratory results. The temperature of T_1 and T_2 is increased from 306 K to 326 K and 301 K to 322 K respectively since the beginning of the mission. The 20 K temperature rise was not sufficient to explain the disagreement on the error budget between the space observations and the laboratory experiment.

The uncertainty on the short term solar irradiance variation is $\pm 0.45\,W\,m^{-2}$ after removing the terrestrial radiation (Zhu et al., 2014). It hints at the fact that the larger error bar deduced from MES could be due to the contribution of terrestrial radiation that was permanently recorded by BOS during entire mission. It proofs that we are able to improve the relative uncertainty, but obviously not the absolute accuracy. On the other hand, the errors on the difference temperature measurements ($T_1 - T_2$) is in miliKelvin calculated both from Laboratory and space experiments. It evidences that the ECM and ambient thermal noise is efficiently reduced with the design of electronic and the thermal structure of BOS instrument.

Globally, the BOS shows a linear degradation of $-16.8 \pm 0.4\,W\,m^{-2}\,yr^{-1}$ ($-33.7\,ppm \pm 0.8\,ppm\,day^{-1}$ to the TSI amount). It is one order higher than the degradation of PMO6V and DIARAD absolute radiometer onboard the SOHO satellite (Fröhlich et al., 1997). The high degradation rate could be linked to the longer exposure time. A robust relation between the exposure time and the detector's degradation could be established when the UV dose can be simultaneously monitored.

The instruments sensitive mode of the absolute radiometer is better modeled with a hyperbolic function. However, from the current space cumulated data, the linear regression function is the best fit for the change of BOS' sensitivity. Taking into account the main detector either of the BOS or the absolute radiometer are black coated, it

GID
4, 627–651, 2014

suggests the nonlinearity of the absolute radiometer's degradation is mainly induced by the optical part rather than the painting. A phenomenon which is attributed as the "siliconizing" of the quartz window exposed when it has a quartz window to UV radiation (Fröhlich, 2003).

The BOS is a perfect Lambertian detector. A cosine correction must be applied to the total number of radiation. The contribution is small since the pointing angle is stable to the Sun direction. The correction is more important for the terrestrial radiation where the pointing angle between the source and the sensor is bigger.

The Bolometeric Oscillation Sensor is a TRL level-9 space instrument after its successful service to the PICARD mission according to the definition of ESA's technology readiness level (ESA, 2012). The details of the instrument is listed at Table 3. The space performance of the instrument proof the BOS is able to measure a large dynamic range of electromagnetic radiation with a relative high resolution. The electronic and thermal design shows its high efficiency to reduce the ECM and ambient thermal noise. The BOS is a stable sensor to track the small amount of variation in the electromagnetic radiation. It can be payload on the micro even cubesat missions to study the irradiance from the solar as well as planetary origin.

Acknowledgements. The comments given by the anonymous reviewers have help us improving the quality of the paper. PICARD mission is supported by Centre National d'Etudes Spatiales (CNES), the CNRS/INSU, the Belgian Space Policy (BELSPO), the Swiss Space Office (SSO), and the European Space Agency (ESA). We would like to thank to Ali Ben Moussa and Boris Giordanengo from the DeMeLab, ROB, who has provided us the Labsphere and source calibration. Marie Dominique for her valuable comments on the manuscript. Frédéric Clette has gave valuable suggestion for data analysis. Jean-Pierre De Cuyper has welcomed us to do the experiment at his digital laboratory. The BOS experiment is financed by Belgian-PRODEX program, ESA project with the management support of BELSPO.

GID
4, 627–651, 2014

References

Dewitte, S., Crommelynck, D., Mekaoui, S., and Joukoff, A.: Measurement and uncertainty of the long-term total solar irradiance trend, Sol. Phys., 224, 209–216, 2004. 628

ESA: Strategic readiness level, available at: http://sci.esa.int/sre-ft/37710-strategic-readiness-level/ (last access:27 November 2014), 2012. 638

Fröhlich, C.: Long-term behaviour of space radiometers, Metrologia, 40, 1–6, 2003. 638

Fröhlich, C., Crommelynck, D. A., Wehrli, C., Anklin, M., Dewitte, S., Fichot, A., Finsterle, W., Jiménez, A., Chevalier, A., and Roth, H.: In-flight performance of the Virgo solar irradiance instruments on SOHO, Sol. Phys., 175, 267–286. doi:10.1023/A:1004929108864, 1997. 636, 637

K&K Associate: Thermal network modeling handbook, Version 97.003, available at: http://www.tak2000.com (last access: 27 November 2014), 2000.

Kopp, G. and Lean, J. L.: A new, lower value of total solar irradiance: evidence and climate significance, Geophys. Res. Lett., 38, 1706, doi:10.1029/2010GL045777, 2011. 636

Labsphere: Uniform source spheres(PB-13019-000), available at: http://www.labsphere.com (last access: 27 November 2014), 2005. 632

Martinez, L. D.: Participation à la conception et à la réalisation du capteur BOS destiné à mesurer la variabilité de l'irradiance solaire totale, thesis, Annee Academique, 2006–2007, Université Libre de Bruxelles, 2007. 630

Measurement specialties: Mini BetaCURVE Thermistor Probe (MDB), available at: http://www.meas-spec.com (last access: 27 November 2014), 2005. 631

Meftah, M., Hochedez, J.-F., Irbah, A., Hauchecorne, A., Boumier, P., Corbard, T., Turck-Chièze, S., Assus, P., Bertran, E., Bourget, P., Buisson, F., Chaigneau, M., Damé, L., Djafer, D., Dufour, C., Etcheto, P., Ferrero, P., Hersé, M., Marcovici, J.-P., Meissonnier, M., Morand, F., Poiet, G., Prado, J.-Y., Renaud, C., Rouanet, N., Rouzé, M., Salabert, D., and Vieau, A.-J.: PICARD SODISM, a space telescope to study the Sun from the middle ultraviolet to the near infrared, Sol. Phys., 289, 1043–1076, 2014a. 629

Meftah, M., Dewitte, S., Irbah, A., Chevalier, A., Conscience, C., Crommelynck, D., Janssen, E., and Mekaoui, S.: SOVAP/Picard, a spaceborne radiometer to measure the total solar irradiance, Sol. Phys., 289, 1885–1899, 2014b. 629, 635

GID
4, 627–651, 2014

Mekaoui, S., Dewitte, S., Conscience, C., and Chevalier, A.: Total solar irradiance absolute level from DIARAD/SOVIM on the International Space Station, Adv. Space Res., 45, 1393–1406, 2010. 628

Miller, R.: DuPont Engineering Technical Information, Polymeres, Vespel polyimide parts and shapes, 2000, available at: http://www.dupont.com (last access: 27 November 2014), 2000. 632

Schmutz, W., Fehlmann, A., Finsterle, W., Kopp, G., and Thuillier, G.: Total solar irradiance measurements with PREMOS/PICARD, AIP Conf. Proc. 1531, 6–10 August 2012, Berlin, 844, doi:10.1063/1.4804902, 2013. 629

Thullier, G., Dewitte, S., Schmutz, W., and The Picard team: Simultaneous measurement of the total solar irradiance and solar diameter by the PICARD mission, Adv. Space Res., 38, 1792–1806, doi:10.1016/j.asr.2006.04.034, 2006. 628

van Ruymbeke, F.: Mise au point d'un capteur embarqué sur satellite destiné à mesurer les variations du flux radiative solaire, thesis, Annee Academique 2005–2006, Université Catholique de Louvain, 2006. 629

van Ruymbeke, M., Renders, F., Noël, J.-P., van Ruymbeke, F., Martinez, D. L., and Zhu, P.: Mise en orbite d'un bolomètre élaboré à l'Observatoire Royal de Belgique 1ère Partie: description du dispositif, Ciel et Terre, 126, 173–179, 2010. 628, 631

van Ruymbeke, M., Zhu, P., Renders, F., and Noël, J.-P.: Mise en orbite d'un bolomètre élaboré à l'Observatoire Royal de Belgique 2ème partie: Présentation d'observations de divers phénomènes enregistrés en orbite par le BOS, Ciel et Terre, 127, 14–16, 2011. 628

Zhu, P., Ruymbeke, M. V., Meftah, M., Clette, F., Dewitte, S., Chevalier, A., van Ruymbeke, F., and Noel, J.: The preliminary measurements from the Bolometer Oscillation System (BOS) on board PICARD, American Geophysical Union, AGU Fall meeting, 13–17 December 2010, San Francisco, California, USA, abstract #GC21B-0873, 2010. 629

Zhu, P., Karatekin, Ö., Noël, J.-P., van Ruymbeke, M., and Dehant, V.: EGU General Assembly 2012, 22–27 April 2012, Vienna, Austria, p. 7271, 2012. 632

Zhu, P., Karatekin, Ö., van Ruymbeke, M., Dewitte, S., and Thuillier, G.: The solar irradiance registered at a flat-hemispherical field of view-bolometric oscillation sensor on board PICARD satellite, EGU2014-5112, EGU General Assembly 2014, Vol 16, 27 April–2 May 2014, Vienna, Austria, 2014. 637

GID

4, 627–651, 2014

A high dynamic radiation measurements instrument

P. Zhu et al.

Table 1. Laboratory experiment results.

Experiment	T_1 (K)	1σ	T_2 (K)	1σ	$T_1 - T_2$ (K)	1σ	F ($W m^{-2}$)	1σ
1	294.888	0.005	294.469	0.004	0.423	0.001	472.6	0.08
2	294.906	0.004	294.482	0.005	0.423	0.001	472.8	0.09
3	294.904	0.010	294.487	0.007	0.423	0.002	472.9	0.10
4	294.909	0.008	294.494	0.003	0.423	0.001	472.9	0.10
5	294.884	0.010	294.473	0.003	0.423	0.002	472.7	0.09
6	294.880	0.009	294.465	0.005	0.423	0.001	472.8	0.10
7	294.891	0.007	294.471	0.006	0.423	0.001	472.8	0.09
8	294.911	0.006	294.495	0.002	0.424	0.001	472.9	0.10

GID
4, 627–651, 2014

Table 2. MES calibration validation.

Date	T_1 (K)	1σ	T_2 (K)	1σ	$T_1 - T_2$ (K)	1σ	F (W m^{-2})	1σ
6 Oct 2010	299.4	0.13	301.4	0.13	−2.226	0.0091	1411.9	0.65
9 Nov 2010	301.8	0.13	303.6	0.13	−2.256	0.0068	1388.0	0.43
4 May 2011	302.7	0.09	304.8	0.12	−2.286	0.0037	1389.5	0.77
30 May 2011	302.4	0.19	304.5	0.11	−2.278	0.0040	1370.9	4.70
1 Oct 2011	305.4	0.14	307.5	0.14	−2.379	0.0036	1371.5	0.86
24 Oct 2011	305.9	0.12	308.1	0.13	−2.381	0.0036	1378.6	0.49
19 Mar 2012	306.5	0.13	308.7	0.13	−2.388	0.0031	1372.0	1.19
24 Mar 2012	306.4	0.13	308.6	0.13	−2.386	0.0037	1371.5	2.59
24 Apr 2012	305.7	0.13	307.8	0.14	−2.362	0.0080	1365.2	3.62
25 May 2012	304.4	0.10	306.5	0.13	−2.323	0.0023	1369.7	1.88
15 Jul 2012	304.5	0.13	306.6	0.13	−2.318	0.0103	1351.7	5.15
22 Jul 2012	304.7	0.13	306.8	0.13	−2.331	0.0077	1355.2	2.57
13 Oct 2012	307.2	0.13	309.4	0.13	−2.419	0.0078	1361.8	1.04
19 Oct 2012	307.4	0.13	309.6	0.13	−2.419	0.0087	1368.7	0.83
9 Nov 2012	308.1	0.15	310.1	0.15	−2.422	0.0068	1343.7	0.30
11 Mar 2013	308.4	0.13	310.5	0.14	−2.424	0.0096	1360.4	0.91
31 Oct 2013	308.6	0.12	310.8	0.13	−2.444	0.0037	1354.7	0.71

GID
4, 627–651, 2014

Table 3. Instrument data sheet.

Parameter	data
Mass (g)	168
Volume (cm^3)	366.7
Height (cm)	9.13
White surface (cm)[a]	6.34
Black surface (cm)[a]	4.65
Shunt (cm)[a]	1.81
Absolute temperature (K)[b]	10^{-1}
Relative temperature (K)[b]	10^{-3}
Flux ($W\,m^{-2}$)[b]	10^{0}
Operating temperature (°C)	[−30 +60]
Power consumption (mW)	[100 300]

[a] Diameter,
[b] sensibility.

GID
4, 627–651, 2014

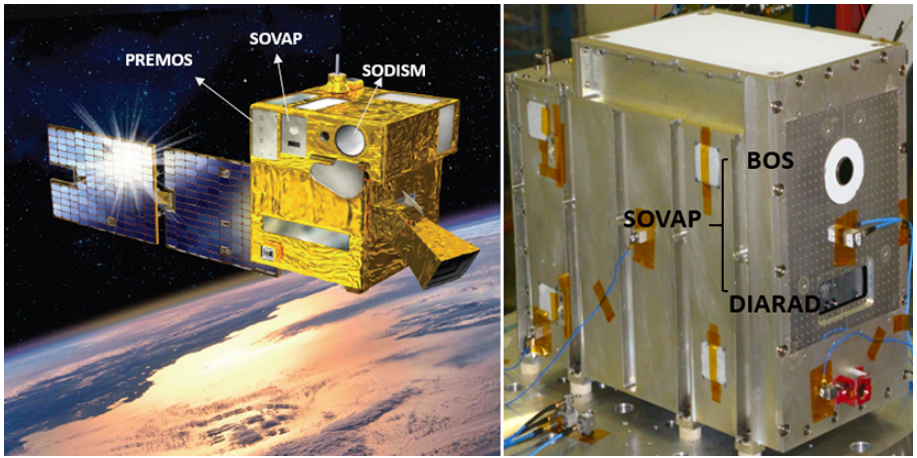

Figure 1. The PICARD satellite and SOVAP experiment. The BOS is integrated in the same unit with DIARAD (photo credits CNES).

GID
4, 627–651, 2014

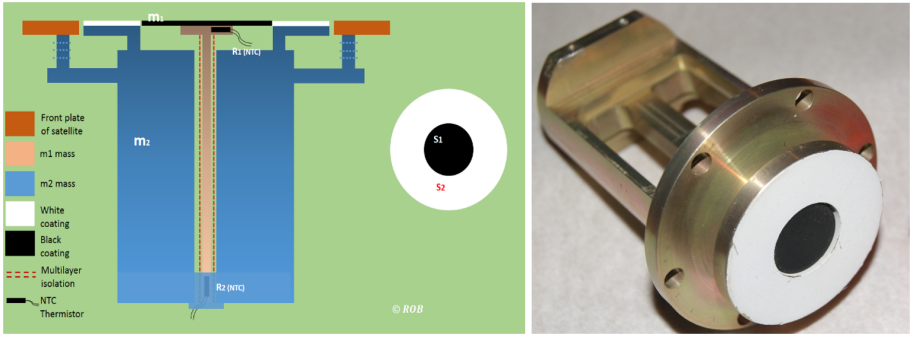

Figure 2. The sketch of BOS. The detector (m_1) is connected to the heat sink (m_2) by a thin shunt, which is thermally isolated from m_2 by multi-layer-isolation (MLI). The instrument unit is installed in the front panel of the spacecraft through a high thermal resistance Vespel® layer.

GID
4, 627–651, 2014

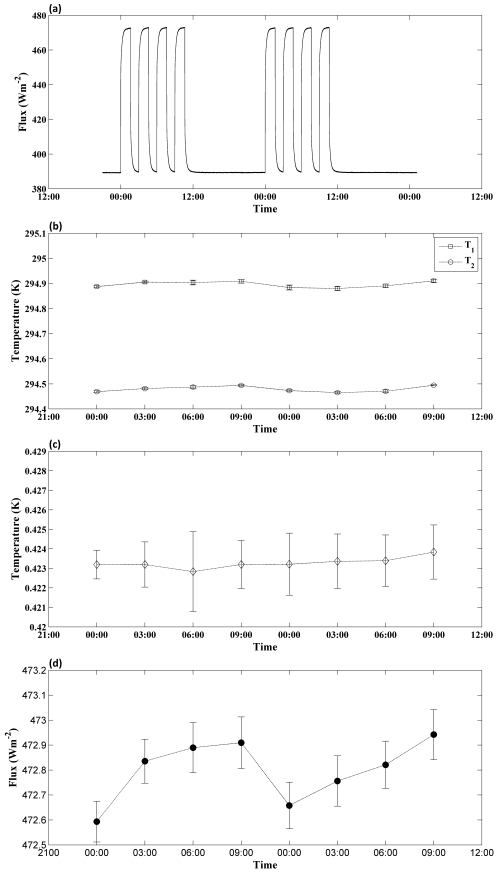

Figure 3. The instrument was tested under a temperature controlled clean room, **(a)** eight cycles of on/off radiation source, **(b)** temperature of T_1 and T_2 measured around the peak of each cycle, **(c)**, the difference temperature $T_1 - T_2$, **(d)**, flux computed from temperature T_1 and T_2.

GID
4, 627–651, 2014

A high dynamic radiation measurements instrument

P. Zhu et al.

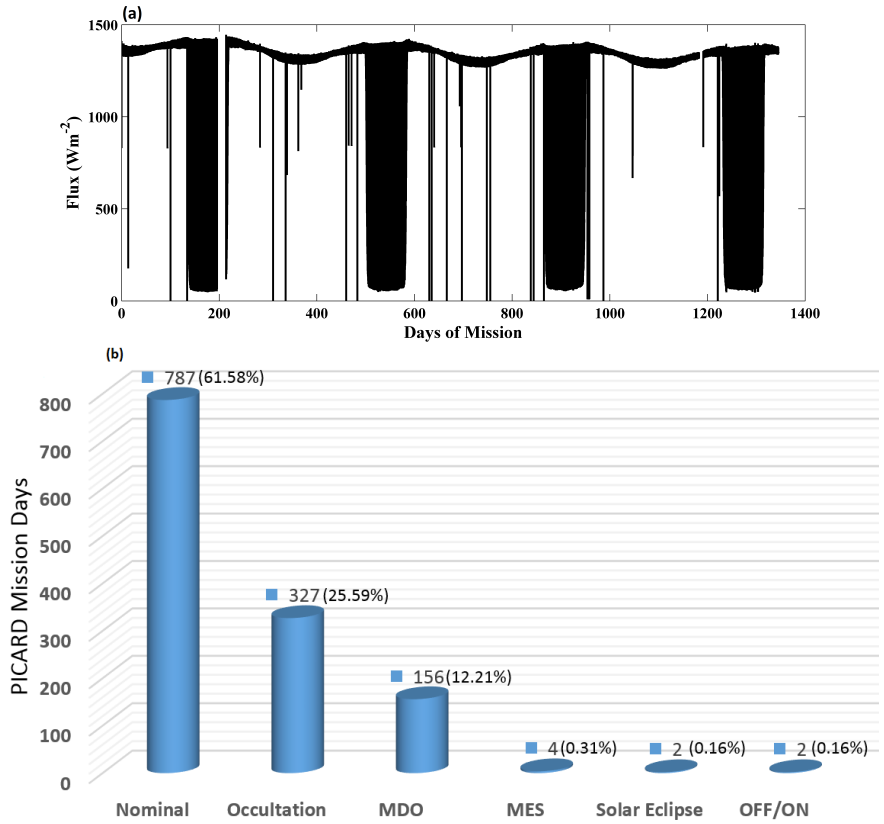

Figure 4. Observations during the entire PICARD mission, **(a)** Level 2 thermal flux, **(b)** data partition according to its physical origin, unit is the day, nominal: is the measurements without any special operation, occultation: observation during the satellite occultation by Earth it is related to the orbit of PICARD, MDO: MOde Distortion, the satellite is rotating along its sun pointing axis, MES: ModE Stellar, the sun pointing axis is turning away to a star, OFF/ON, SOVAP experiment is switch off and on to test the electrical ground.

GID
4, 627–651, 2014

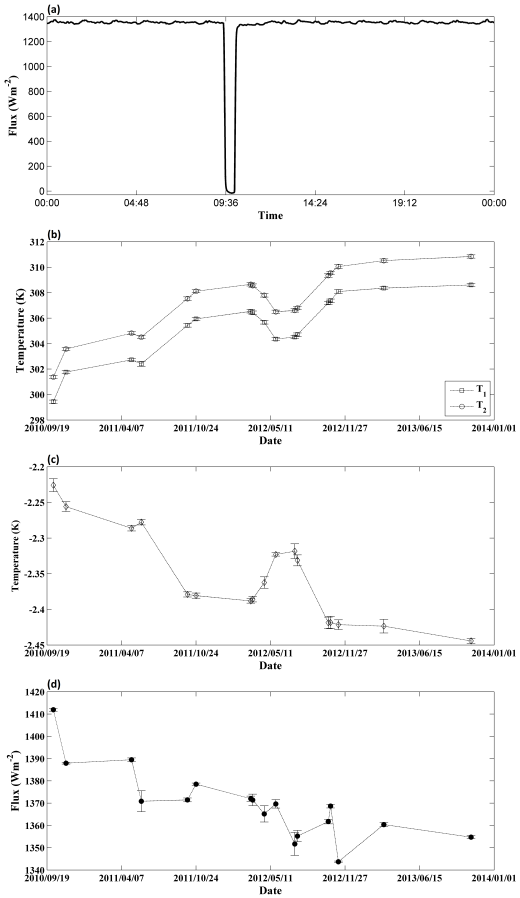

Figure 5. Star pointing events(MES) observed in space, **(a)** one examples of MES events **(b)** T_1 and T_2 of all MES, **(c)** the difference temperature ($T_1 - T_2$) **(d)** The calibrated flux, it has been normalized to 1 AU.

GID
4, 627–651, 2014

A high dynamic radiation measurements instrument

P. Zhu et al.

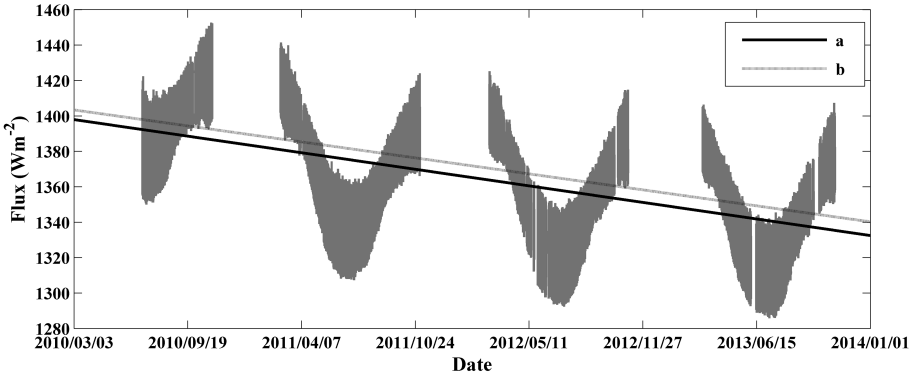

Figure 6. Decrease of the instrument sensitivity as obtained from the global dataset **(a)** and from MES **(b)**.

GID
4, 627–651, 2014

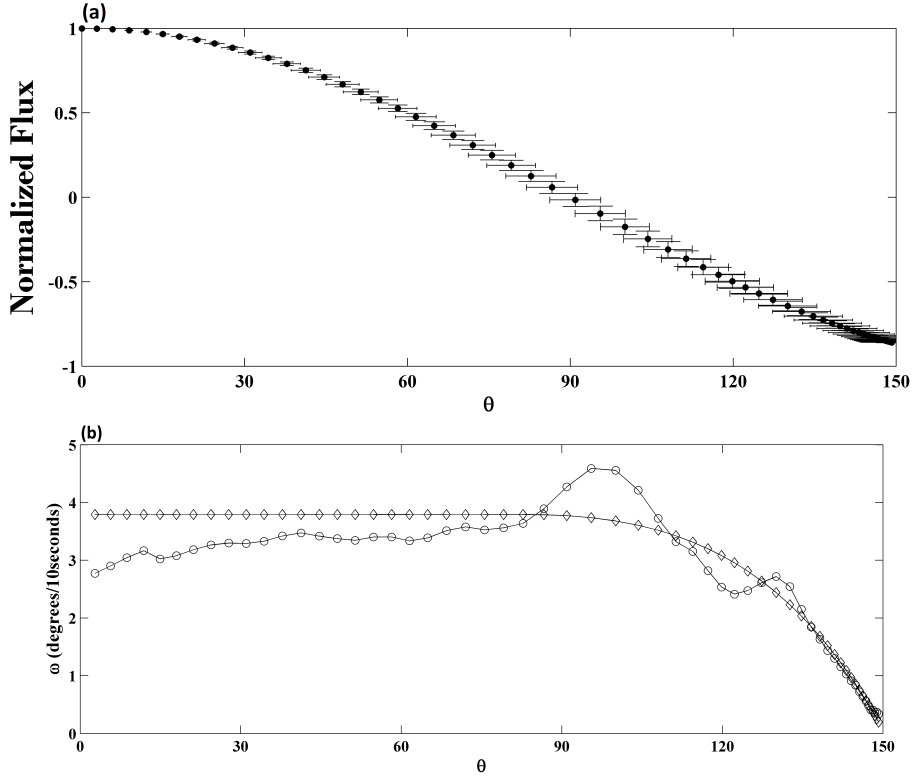

Figure 7. Upper panel, stacking results of 17 star pointing (MES) observations during ascending phases. Lower pane, the diamond sign is the rotation of the spacecraft, the circle is repenting the motion inverted from BOS records.

GID
4, 627–651, 2014

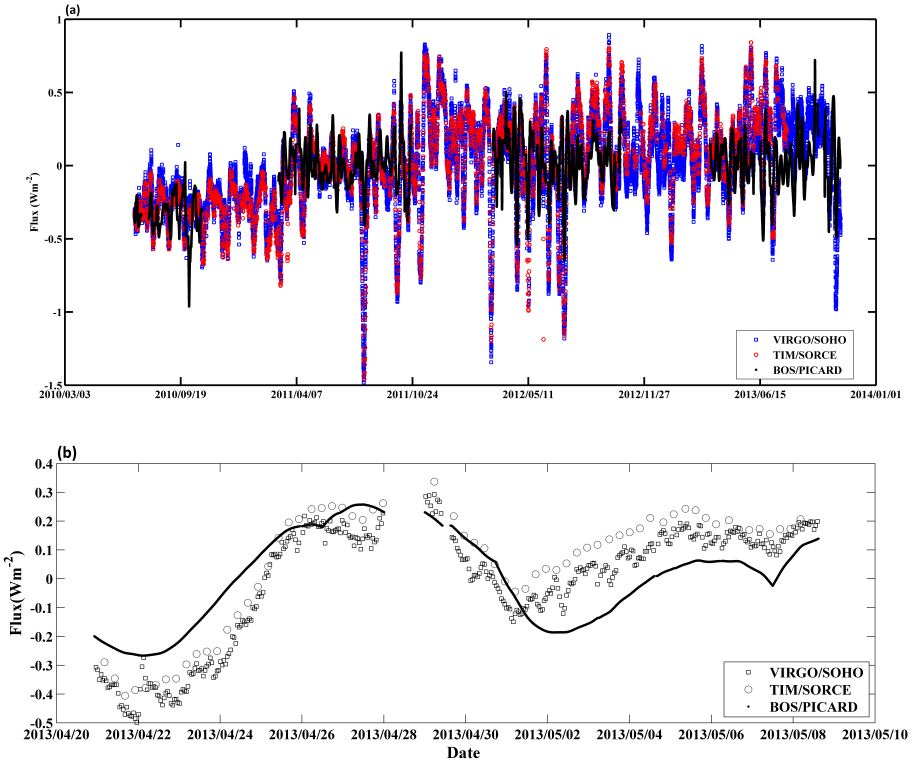

Figure 8. Comparison of BOS with VIRGO/SOHO and TIM/SORCE. Upper panel the records during whole PICARD life time. The cross correlation is BOS-VIRGO: 60.3 %, BOS-TIM: 61.7 %, VIRGO-TIM: 97.5 %. Lower panel a zoom in of upper panel, the three measurements are plotted together with the sampling periods of 10 s for BOS, 1 h for VIRGO and 6 h for TIM. The cross-correlation coefficient over this perod are BOS-VIRGO: 66.5 %, BOS-TIM: 62.3 %, VIRGO-TIM, 90.5 %.

GID
4, 627–651, 2014